Int. J. Heat Mass Transfer. Vol. 30, No. 7, pp. 1497–1509, 1987
Printed in Great Britain

0017-9310/87 $3.00 + 0.00
Pergamon Journals Ltd.

Numerical solution for film evaporation of a spherical liquid droplet on an isothermal and adiabatic surface†

T. K. NGUYEN
Department of Chemical Engineering, California State Polytechnic University, Pomona, CA 91768, U.S.A.

and

C. T. AVEDISIAN
Sibley School of Mechanical and Aerospace Engineering, Cornell University, Ithaca, NY 14853, U.S.A.

(*Received* 25 *August* 1986 *and in final form* 14 *January* 1987)

Abstract—A numerical solution for the problem of film evaporation of a liquid droplet on a horizontal surface is presented. The droplets are small enough to be assumed spherical. Two principal cases are considered: (1) the horizontal surface is maintained at a constant temperature (case I), and (2) the surface is insulated while the ambience is hot (case II). The complete set of equations governing this problem were solved under the following assumptions: (1) evaporation is quasi-steady, (2) no internal liquid circulation, (3) constant properties, and (4) the droplet temperature is spatially uniform but temporally varying. The Lewis number is not assumed to be unity; gas phase viscous effects, Stefan type convection, and gas phase inertia are included in the analysis. The total droplet evaporation time was found to decrease with increasing plate (I) or ambient (II) temperature as expected, and the droplet progressively moves away from the plate as it evaporates. The numerical results agree with the analytical solution for film evaporation of a droplet above an adiabatic surface in a hot ambience in the limit of large effective Reynolds number (i.e. potential flow).

1. INTRODUCTION

THIS paper presents a numerical solution to the problem of Leidenfrost evaporation. The most elementary configuration is treated here, namely that of an isolated spherical droplet evaporating at a horizontal surface. The intent is to develop a predictive framework for the evolution of droplet size and temperature for droplets evaporating at walls. The analysis may be a first step toward developing a complete model of the interaction of droplets in a spray with the walls of a combustor.

Prior work on the film evaporation of liquid droplets at walls has been pursued from both experimental and semi-empirical viewpoints. Experimental work has employed a variety of pure liquids, mixtures, emulsions, and solid suspensions on impermeable and porous materials. Other approaches of a more analytical nature have either simplified the droplet geometry, governing equations, or fluid flow patterns to provide formulations which nevertheless have been useful in correlating evaporation time measurements and in providing insight into the physics of the evaporation process (e.g. see refs. [1–11]). However, full solutions to the governing equations which avoid the approximations of previous work, in particular those of the geometry, heat transfer, and vapor flow surrounding the droplet, have not been presented.

The primary difficulty in obtaining a solution is in the complexity of the governing equations written in an orthogonal coordinate system for which the coordinate axes coincide with the droplet and the wall. The problem is further complicated by the fact that simplifications to the equations which would be obvious candidates for a first attempt at closed form solutions, namely those of either a Stokes type flow in the vapor surrounding the droplet coupled with conduction only in the gas phase, or the other extreme of potential flow, would not be valid. This fact may be seen by noting that in analogy with droplet evaporation in an unbounded environment far from the critical point, the gas phase Reynolds number is approximately

$$Re \sim \frac{\ln(1+B)}{Pr} = O(1) \tag{1}$$

where the Prandtl number, Pr, is also of order unity and B is the so-called transfer number [12]. Thus both the inertia and viscous terms would have to be retained in the momentum equation. Also, the Peclet number

$$Pe \equiv Re\,Pr \tag{2}$$

is then of order unity so that the convective term in

† Part of this paper was presented at the 1987 ASME–JSME Thermal Engineering Joint Conference, Honolulu, 23–27 March 1987.

NOMENCLATURE

A	scale factor (Fig. 1)
B	transfer number
C_v	vapor specific heat
C_l	liquid specific heat
d	droplet diameter
D	binary gas diffusion coefficient
g	gravitational constant
h_1, h_2, h_3	metric coefficients
h_{fg}	latent heat of vaporization
$\mathbf{j}$	unit vector in vertical direction
k	gas thermal conductivity
$\mathbf{n}$	unit outward normal to droplet
$\mathbf{n}_\alpha$	unit vector in α-direction
$\mathbf{n}_\beta$	unit vector in β-direction
P	pressure
R	droplet radius
t	time
T_∞	ambient temperature
T_p	plate temperature
T_s	droplet temperature
u_α	velocity component in α-direction
u_β	velocity component in β-direction
$\mathbf{V}$	velocity vector
V_n	normal velocity at solid surface
v	droplet volume
Y_i	mass fraction of species i
Y_{1s}	mass fraction of vapor at droplet surface.

Greek symbols

α	principal bispherical coordinate
α_v	gas thermal diffusivity
β	principal bispherical coordinate
β_0	coordinate corresponding to droplet
γ	gas emissivity
δ	levitation height
η	transformed coordinate
μ_v	dynamic viscosity
ν	gas kinematic viscosity
ξ	vorticity
Π	total stress tensor
ρ_v	gas density
ρ_l	liquid density
σ	droplet surface area
Σ	Stefan–Boltzmann constant
ϕ	velocity potential
ϕ_1	velocity potential at droplet surface
ψ	stream function.

the energy equation cannot be dropped. The value of such approximations in the present problem is in the checks they can provide on the accuracy of the numerical method employed for solving the full set of equations when the limiting approximations are made. The potential flow solution, in particular, is used in this way (see Appendix A).

Two principal cases are considered. In the first the horizontal surface is maintained at a constant temperature (case I), and in the second the horizontal surface is insulated while the ambience is hot (case II). The droplet shape is taken to be spherical rather than sessile in the present analysis (which is relevant to droplets typically found in industrial sprays, and valid for small droplets generally less than 100 μm in diameter [13]). Several additional assumptions are as follows: (1) the evaporation process is quasi-steady, (2) fluid properties are constant, (3) radiative effects are negligible, (4) spatial nonuniformities of temperature within the droplet are neglected, and (5) buoyancy induced flow and internal liquid motion within the droplet are neglected (see Appendix B).

Radiative effects are negligible provided the analysis is restricted to low plate (case I) or ambient (case II) temperatures such that for example (case I) $\Sigma\gamma(T_p^4 - T_s^4)/(k(T_p - T_s)/\delta) \ll 1$. Though gas phase properties are considered uniform in this analysis, we do include the variations of liquid density and specific heat with temperature to treat the transient heating period. We consider the simplest model for droplet heating, namely that the droplet temperature is spatially uniform but temporally varying. Finally, the Lewis number is not assumed to be unity, and gas phase viscous and inertia effects, and Stefan type convection, are included in the analysis.

2. FORMULATION

A single component liquid droplet in an inert ambience starts evaporating above a horizontal surface. Vapor flows radially outward from the droplet, and the corresponding streamlines bend due to the presence of the wall. A pressure field is thus created around the droplet, and the component of this field normal to the surface lifts the droplet off the surface. This state of levitation persists until the droplet completely evaporates. The problem is to determine the evolution of the velocity and temperature fields in the gas surrounding the droplet, levitation height, and droplet diameter.

The equations to be solved are as follows:

$$\text{continuity} \qquad \nabla\cdot\mathbf{V} = 0 \tag{3}$$

$$\text{momentum} \qquad \mathbf{V}\cdot\nabla\mathbf{V} = -\frac{1}{\rho_v}\nabla P + \frac{\mu_v}{\rho_v}\nabla^2\mathbf{V} \tag{4}$$

$$\text{energy} \qquad \mathbf{V}\cdot\nabla T = \alpha_v\nabla^2 T \tag{5}$$

$$\text{species} \qquad \mathbf{V}\cdot\nabla Y_i = D\nabla^2 Y_i \tag{6}$$

where $i = 1$ (droplet) or 2 (inert ambient) and

$Y_1 + Y_2 = 1$. A force balance on the levitated droplet equates the droplet weight with the net force acting on the droplet (sum of viscous shear and normal stresses, and pressure forces)

$$\int \mathbf{j} \cdot \Pi \, d\sigma = \mathbf{g}(\rho_l - \rho_v)v \tag{7}$$

where Π is the total stress tensor and $\mathbf{j}$ is the unit vector in the vertical direction. In the problem considered the ambience was a single component inert gas (air) and the droplet was a single component liquid (water or n-heptane). By writing the force balance in the form of equation (7) we neglect effects of droplet acceleration caused by variations in levitation height in this first phase of our work.

The boundary conditions are as follows:

solid surface

$$\mathbf{V} = 0 \tag{8a}$$

$$\frac{\partial V_n}{\partial n} = \frac{\partial Y_1}{\partial n} = 0 \tag{8b}$$

$$\tag{8c}$$

$$T = T_p \quad \text{(case I)} \tag{8d}$$

$$\frac{\partial T}{\partial n} = 0 \quad \text{(case II)}$$

droplet surface

$$T = T_s \tag{9a}$$

$$Y = Y_{ls} \tag{9b}$$

ambience

$$\mathbf{V} \to 0 \tag{10a}$$

$$Y_l \to 0 \tag{10b}$$

$$T \to T_\infty. \tag{10c}$$

Equations (3)–(10) were first cast in the bispherical coordinate system (Fig. 1). This coordinate system consists of a family of spheres (β = constant) which are each orthogonal to a family of spindle shaped surfaces (α = constant). A droplet is the sphere $\beta = \beta_0$ and the solid surface corresponds to $\beta = 0$. The scale factor 'A' is given by

$$A = R \sinh \beta_0 \tag{11}$$

and the levitation height, δ, is

$$\delta = R(\cosh \beta_0 - 1). \tag{12}$$

Equations (3)–(10) are now written in the so-called stream function (ψ)/vorticity (ξ) form. Equations (3) and (4) transform to [14]

$$\xi = \frac{1}{h_1 h_2}\left\{\frac{\partial}{\delta\alpha}\left(\frac{h_2}{h_3 h_1}\frac{\partial \psi}{\partial \alpha}\right) + \frac{\partial}{\partial \beta}\left(\frac{h_1}{h_2 h_3}\frac{\partial \psi}{\partial \beta}\right)\right\} \equiv \frac{1}{h_3}E^2\psi \tag{13}$$

and

$$\frac{1}{h_1 h_2 h_3}\frac{\partial(\psi, E^2\psi)}{\partial(\alpha, \beta)} - \frac{2E^2\psi}{h_1 h_2 h_3^2}\frac{\partial(\psi_1 h_3)}{\partial(\alpha, \beta)} = vE^4\psi. \tag{14}$$

The operator E^2 is defined as

$$E^2 = \frac{h_3}{h_1 h_2}\left\{\frac{\partial}{\partial \alpha}\left(\frac{h_2}{h_3 h_1}\frac{\partial}{\partial \alpha}\right) + \frac{\partial}{\partial \beta}\left(\frac{h_1}{h_2 h_3}\frac{\partial}{\partial \beta}\right)\right\}. \tag{15}$$

Using the definition of E^2, equation (14) can be rewritten as

$$\frac{1}{h_1 h_2 h_3}\frac{\partial(\psi, h_3\xi)}{\partial(\alpha, \beta)} - \frac{2\xi}{h_1 h_2 h_3}\frac{\partial(\psi, h_3)}{\partial(\alpha, \beta)} = vE^2(h_3\xi). \tag{16}$$

The metric coefficients are [15]

$$h_1 = h_2 = \frac{A}{\cosh \beta - \cos \alpha}, \quad h_3 = \frac{A \sin \alpha}{\cosh \beta - \cos \alpha}. \tag{17}$$

The velocity components in the α- and β-direction are

$$u_\alpha = -\frac{1}{h_2 h_3}\frac{\partial \psi}{\partial \beta}, \quad u_\beta = \frac{1}{h_1 h_3}\frac{\partial \psi}{\partial \alpha}. \tag{18}$$

The boundary conditions are

$$\psi = 0 \text{ at } \alpha = 0 \tag{19a}$$

$$\psi = \text{a constant at } \alpha = \pi \tag{19b}$$

$$\psi = \text{a constant at } \beta = 0 \tag{19c}$$

$$\frac{\partial \psi}{\partial \beta} = 0 \text{ at } \beta = \beta_0 \tag{19d}$$

$$\xi = 0 \text{ at } \alpha = 0, \pi. \tag{19e}$$

Similarly the energy equation (equation (5)) is

$$\frac{u_\alpha}{h_1}\frac{\partial T}{\partial \alpha} + \frac{u_\beta}{h_2}\frac{\partial T}{\partial \beta} = \frac{k}{\rho_v C_v}\frac{1}{h_1 h_2 h_3} \times \left\{\frac{\partial}{\partial \alpha}\left(\frac{h_2 h_3}{h_1}\frac{\partial T}{\partial \alpha}\right) + \frac{\partial}{\partial \beta}\left(\frac{h_3 h_1}{h_2}\frac{\partial T}{\partial \beta}\right)\right\} \tag{20}$$

with boundary conditions

$$\frac{\partial T}{\partial \alpha} = 0 \text{ at } \alpha = 0, \pi \tag{21a}$$

$$\frac{\partial T}{\partial \alpha} = 0 \quad \text{(case II)}$$

or

$$\text{at } \beta = 0 \tag{21b}$$

$$T = T_p \quad \text{(case I)}$$

$$T = T_\infty \text{ at } \alpha = \beta = 0. \tag{21c}$$

The transient droplet temperature, $T_s(t)$, is determined from an energy balance at the droplet surface

$$-\int \frac{k}{h_2}\frac{\partial T}{\partial \beta} d\sigma = \int \rho_v h_{fg} u_\beta \, d\sigma + \frac{d}{dt}\left(\frac{4}{3}\pi R^3 \rho_l C_l T_s\right) \tag{21d}$$

where ρ_l and C_l are time dependent through their variations with temperature. The initial condition on droplet temperature is that $T_s = T_{s0}$.

Finally, the species conservation equation (equation (6)) is

$$\frac{u_\alpha}{h_1}\frac{\partial Y_1}{\partial \alpha} + \frac{u_\beta}{h_2}\frac{\partial Y_1}{\partial \beta} = \frac{D}{h_1 h_2 h_3} \times \left\{\frac{\partial}{\partial \alpha}\left(\frac{h_2 h_3}{h_1}\frac{\partial Y_1}{\partial \alpha}\right) + \frac{\partial}{\partial \beta}\left(\frac{h_3 h_1}{h_2}\frac{\partial Y_1}{\partial \beta}\right)\right\} \tag{22}$$

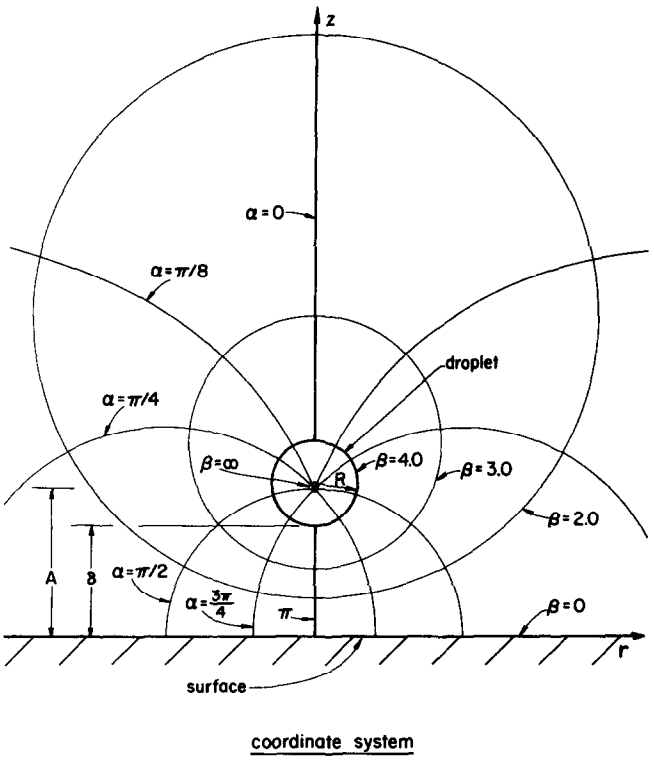

FIG. 1. Coordinate system.

with boundary conditions

$$\frac{\partial Y_1}{\partial \alpha} = 0 \text{ at } \alpha = 0, \pi \tag{23a}$$

$$\frac{\partial Y_1}{\partial \alpha} = 0 \text{ at } \beta = 0 \tag{23b}$$

and

$$\frac{D}{h_2}\frac{\partial Y_1}{\partial \beta} = (1 - Y_{1s})u_\beta \text{ at } \beta = \beta_0. \tag{23c}$$

Y_{1s} is unknown and was obtained from the assumption of vapor/liquid equilibrium at the droplet surface.

The levitation height is determined by equation (7)

$$\int [(-p + \tau_{\beta\beta})\mathbf{n}_\beta + \tau_{\alpha\beta}\mathbf{n}_\alpha] \cdot \mathbf{j}\, d\sigma = \frac{4}{3}\pi R^3 g(\rho_1 - \rho_v) \tag{24}$$

where the stress components at the droplet surface are given by

$$\tau_{\alpha\beta} = -\mu\left\{\frac{(\sinh\beta)u_\alpha}{h_1(\cosh\beta - \cos\alpha)} + \frac{1}{h_1}\frac{\partial u_\beta}{\partial \alpha} + \frac{(\sin\alpha)(u_\beta)}{h_2(\cosh\beta - \cos\alpha)} + \frac{1}{h_2}\frac{\partial u_\alpha}{\partial \beta}\right\} \tag{25}$$

$$\tau_{\beta\beta} = -2\mu\left\{\frac{-(\sin\alpha)u_\alpha}{h_2(\cosh\beta - \cos\alpha)} + \frac{1}{h_2}\frac{\partial u_\beta}{\partial \beta}\right\}. \tag{26}$$

The pressure P is obtained from the momentum equation (equation (4)).

The droplet evaporation time is obtained by integrating the equation

$$\frac{4}{3}\pi\frac{d}{dt}(\rho_1 R^3) = \rho_v \int u_\beta\, d\sigma. \tag{27}$$

The physical properties used in the solution were evaluated at the ambient pressure (0.101 MPa) and at an arithmetic average temperature and concentration between the droplet surface and the ambience (other rules used for evaluating the physical properties did not affect the form of the solution). The temperature and concentration dependence of these properties was obtained from formulations given in ref. [16].

3. METHOD OF SOLUTION

One difficulty of obtaining a solution is the possibility that the moving droplet boundary could reside between adjacent grids in the finite difference scheme. A coordinate transformation which immobilizes the droplet boundary was accordingly used. This transformation is as follows:

$$\eta = \frac{\beta_0 - \beta}{\beta_0} \tag{28}$$

where β_0 is the droplet surface and the domain of the solution is in the range $0 \leqslant \beta \leqslant \beta_0$. The droplet surface is then transformed to a fixed line $\eta = 0$, and the wall is at $\eta = 1$. The α–η plane thus represents a rectangular grid fixed in time. Equations (13)–(27) were written in the α–η system (the results are too lengthy to present), and then put in finite difference form.

The finite differenced equations and boundary conditions were solved using a successive overrelaxation scheme [17]. The iterative solution centered around the levitation height. With R and T_s initially known, a value of δ was selected after which β_0 was determined from equation (12). The conservation equations were then solved for the temperature, velocity, and concentration fields. For this purpose a (21×21) grid was chosen to yield a combination of acceptable accuracy and a reasonable computational time. Appendix B discusses the accuracy of the numerical scheme. Optimum relaxation factors of 1.4 for the stream function, 1.2 for the vorticity, and 1.85 for both the energy and species equation were used. Typical CPU times for one complete evaporation time determination at each preselected ambient (case II) or surface (case I) temperature averaged about 1 h on an IBM 4381. The droplet radius at the next time increment (dimensionally, about 0.2 ms for the present calculations) was then obtained from equation (27), followed by a determination of the new T_s from equation (21e).

The calculations were terminated when the droplet was small enough so that it reached over 90% of its evaporation time. The evaporation time was then inferred by extrapolation to $R = 0$. The reason for this extrapolation is that δ/R rapidly diverges (but is not infinite) as $R \to 0$ so that convergence of the force balance to yield the levitation height becomes particularly difficult to achieve as the droplet size diminishes.

4. DISCUSSION OF RESULTS

Calculations are reported for water and n-heptane droplets initially 50 μm in diameter. Figure 2 shows streamlines around an n-heptane (Fig. 2(a)) and water (Fig. 2(b)) droplet evaporating above an isothermal surface at the start of evaporation ($t = 0$). In all the calculations, $T_{s0} = 300$ K. The streamlines exhibit a form similar to a point source near an infinite plane with streamline curvature providing a measure of the pressure gradient around the droplet. While the streamlines are normal to the droplet surface so that the vapor flow is only in the radial direction there, the tangential velocity gradient will be nonzero. This gradient contributes to the viscous and inertia terms in the momentum equation which, when multiplied by the normal vapor velocity at the droplet, balance the pressure gradient around the droplet surface with the weight of the droplet. The droplets in Fig. 2 were positioned at their levitation height, which was obtained by satisfying equation (24).

The temporal variation of droplet diameter (d^2) is illustrated in Fig. 3. There is a short initial transient period during which the droplet actually grows larger than its initial size. This effect is related to liquid density variations with temperature and is a characteristic of isolated droplet evaporation in an infinite gaseous medium [12]. If the transient heating period is ignored the diameter (d^2) decreases monotonically with time.

During the transient heating period, the droplet temperature approaches a steady state wet-bulb value as shown in Fig. 4. This temperature (338.4 K for an n-heptane droplet corresponding to the conditions of our calculations) is the same for both the case I and case II calculations and is below the n-heptane normal boiling point of 371 K. When the ambient and surface temperatures are the same for cases I and II (which it was for the calculations shown in Fig. 4), the asymptotic wet-bulb temperature will be the same for evaporation above an adiabatic and isothermal surface. Also illustrated in Fig. 4 is that the droplet temperature overshoots its infinite medium wet-bulb temperature when evaporating at an isothermal surface, but asymptotically approaches this value for evaporation at an adiabatic surface (when the ambient temperature is the same for both cases). At an isothermal surface the proximity of the hot surface to the cold droplet results in a higher heat transfer rate compared to a droplet at an adiabatic surface in a hot ambience. As a result, the droplet temperature will be higher for a droplet evaporating at an isothermal surface when boundary temperatures are the same for cases I and II. Eventually, the droplets approach the same steady state wet-bulb temperature as the effect of the wall diminishes because the droplet moves away from the surface as it evaporates. This latter effect is shown in Fig. 5 for a droplet at an isothermal surface. Also illustrated is the effect of the transient heating period on the levitation height. A droplet initially resides closer to the surface when transient heating is accounted for than when the droplet is assumed to already be at its wet-bulb temperature.

The variation of levitation height illustrated in Fig. 5 did not exhibit any periodic or oscillatory behavior. Oscillatory behavior of the calculated levitation height may have been expected based on prior experimental observations for larger sessile shaped drops, even when free convective effects are neglected [7]. The absence of droplet oscillations (i.e. a periodic alternate movement of a droplet toward and away from the surface) in the present calculations may be due to neglecting the acceleration term in the force balance of equation (7) as previously mentioned.

The calculated increase in levitation height with time shown in Fig. 5 is at variance with several previous more approximate models, results from which have shown that a droplet moves toward an isothermal surface as it evaporates (e.g. refs. [1, 2, 4, 11]).

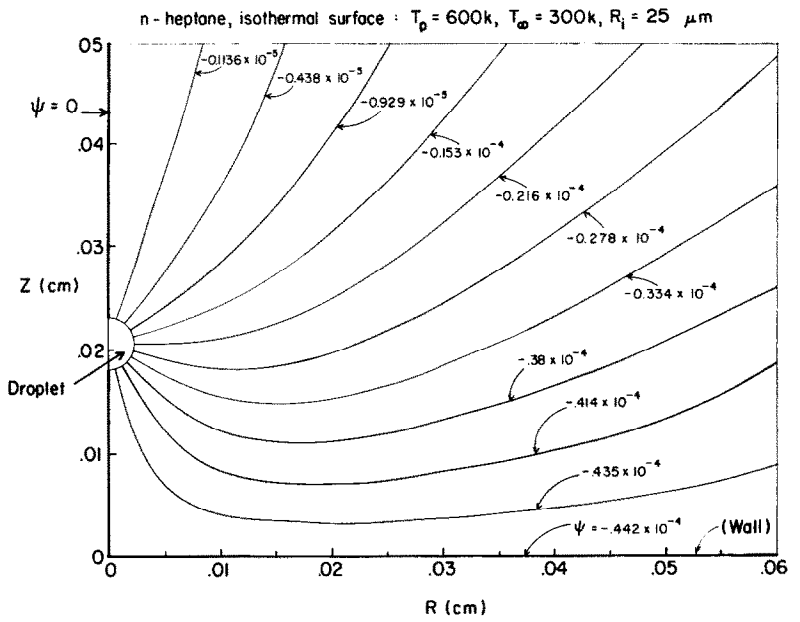

(a)

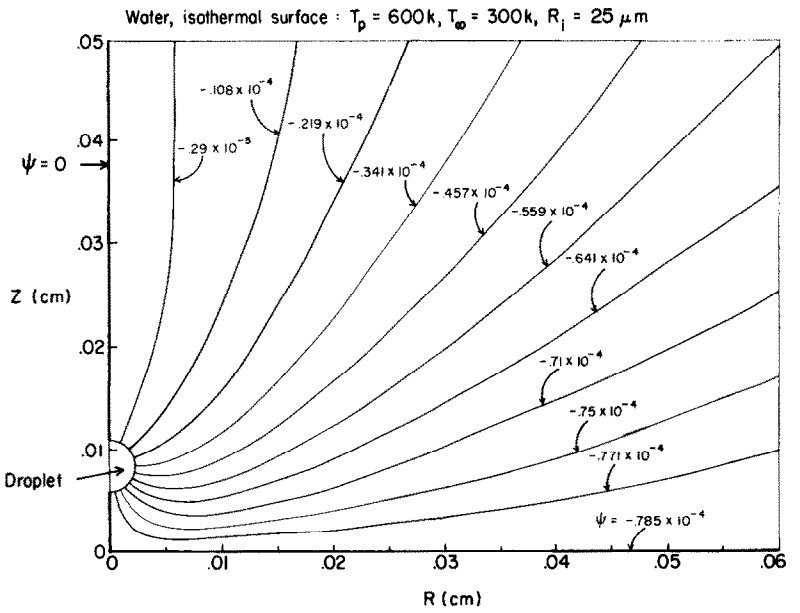

(b)

FIG. 2. Calculated streamlines around an n-heptane (a) and water (b) droplet evaporating in nitrogen.

Though these models have been useful for correlating evaporation time measurements, they have been based on modelling droplets as essentially truncated spheres with flat bases to which heat transfer occurs to the exclusion of evaporation over the upper surface of the droplet. As the droplet gets smaller, the base area rapidly decreases and the droplet must reside closer to the surface to compensate.

Figures 6 and 7 illustrate the variation of the total evaporation time with surface (case I) or ambient (case II) temperature for an n-heptane droplet initially 50 μm in diameter. These calculations are essentially the loci of times corresponding to $d^2 = 0$, obtained by varying the surface or ambient temperature. Calculations were carried out over the temperature range of 500–700 K. The lower limit is above the Leidenfrost point for heptane [8]. Results show that the evaporation time decreases with increasing surface (case I) or ambient (case II) temperature. This fact is in accordance with many previous experimental case I observations for much larger and initially non-spherical droplets; no data have yet been published corresponding to the small initially spherical droplets considered in the present calculations. Also, the

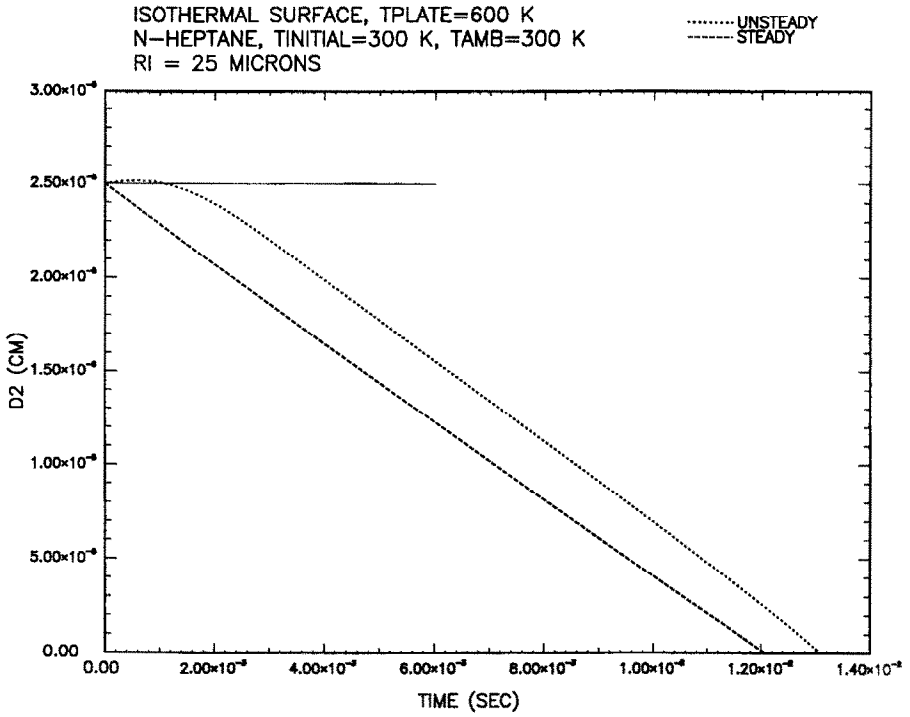

FIG. 3. Variation of d^2 (cm^2) with time (s) for an n-heptane droplet evaporating above an isothermal surface. $T_{s0} = 300\,\text{K}$, $T_\infty = 300\,\text{K}$, $T_p = 600\,\text{K}$, $R_i = 25\,\mu\text{m}$. ----, Steady state. ····, Unsteady state.

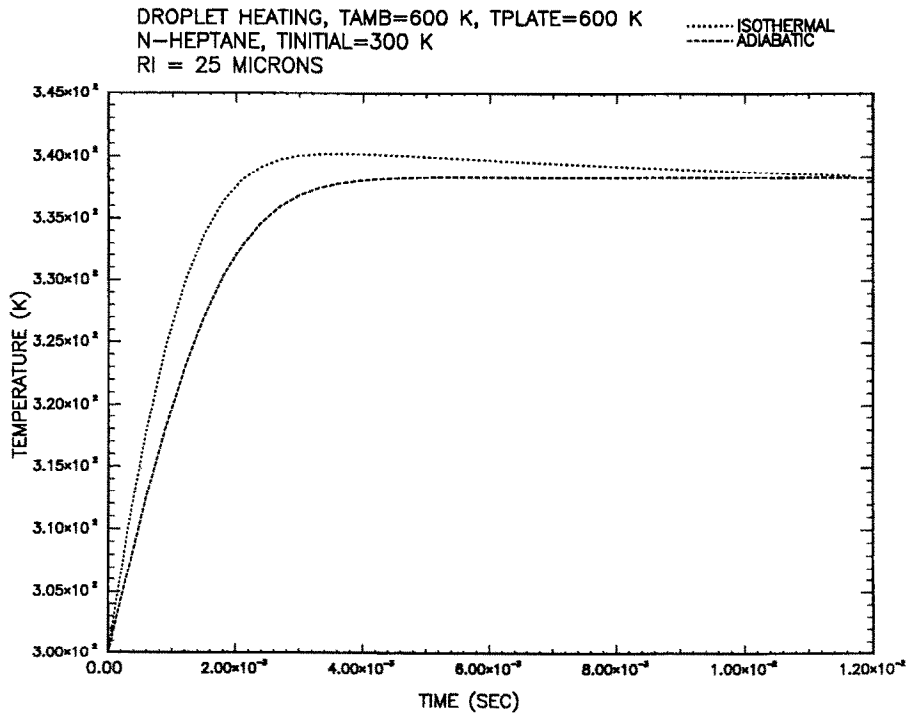

FIG. 4. Temporal variation of droplet temperature, T_s, for n-heptane evaporating above an isothermal (····) or adiabatic (----) surface. $T_{s0} = 300\,\text{K}$, $T_\infty = T_p = 600\,\text{K}$, $R_i = 25\,\mu\text{m}$.

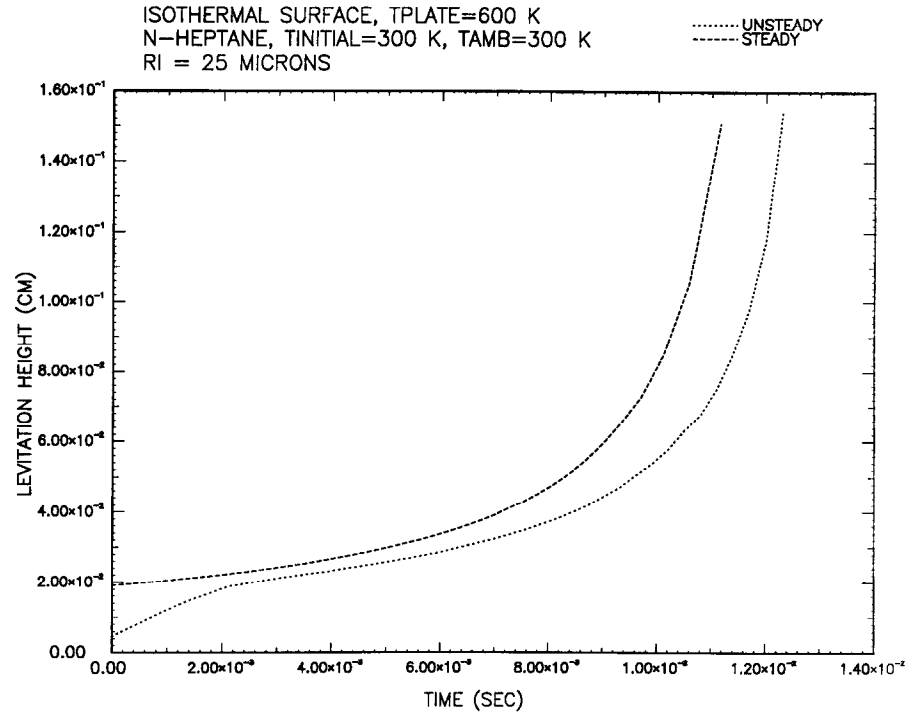

FIG. 5. Variation of levitation height with time for an n-heptane droplet evaporating above an isothermal surface. $T_p = 600$ K, $T_{s0} = T_\infty = 300$ K, $R_i = 25$ μm. ——, Steady state. · · · ·, Unsteady state.

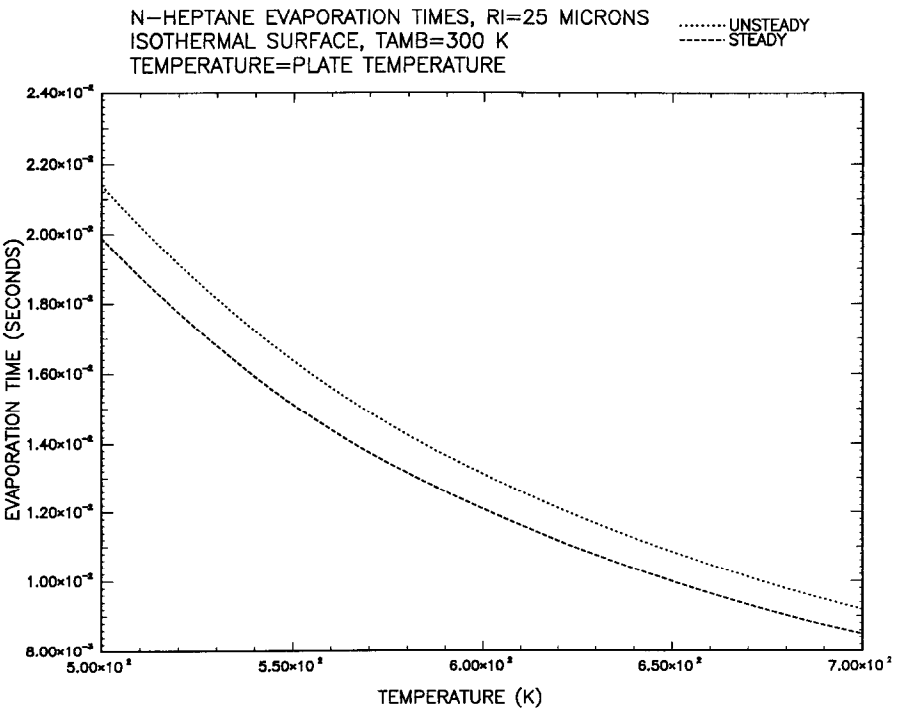

FIG. 6. Effect of plate temperature on total droplet evaporation time for n-heptane at an isothermal surface. $T_{s0} = T_\infty = 300$ K, $R_i = 25$ μm. · · · ·, Unsteady state. ——, Steady state.

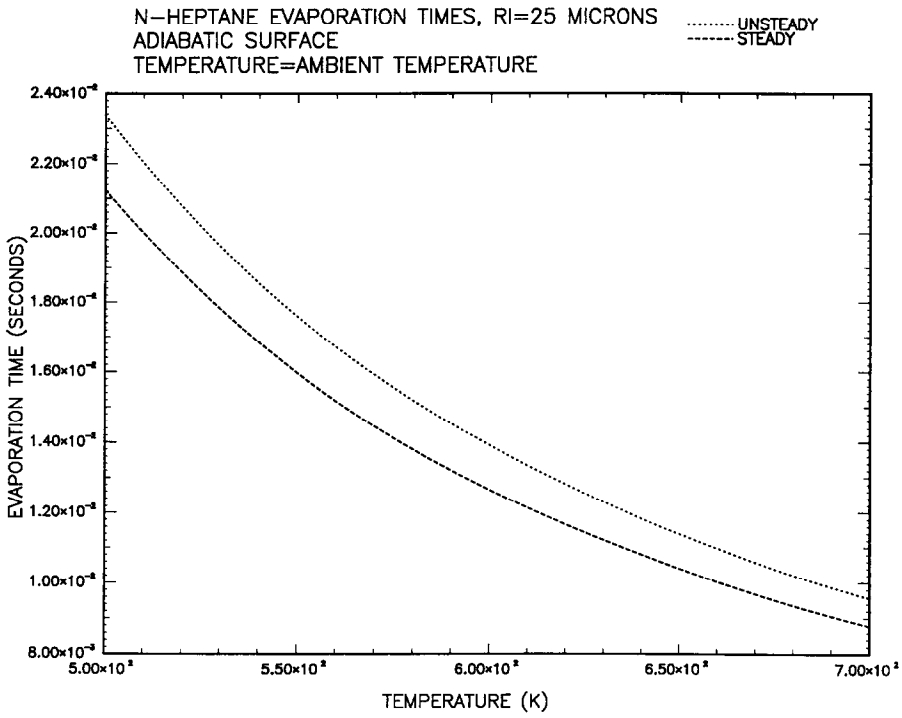

FIG. 7. Effect of ambient temperature on total droplet evaporation time for n-heptane at an adiabatic surface. $T_{s0} = 300\,\text{K}$, $R_i = \mu\text{m}$. ····, Unsteady state. ----, Steady state.

neglect of droplet heating results in a lower evaporation time as expected.

5. CONCLUSIONS

A numerical solution to the problem of Leidenfrost evaporation of isolated spherical droplets has been presented. The results showed that streamlines emanating from a droplet evaporating either above an isothermal (case I) or adiabatic (case II) surface exhibit a form similar to a point source above a plane wall. The total droplet evaporation time progressively decreases as the wall (case I) or ambient (case II) temperature increases, and the evolution of droplet diameter squared may increase above its initial value when droplet heating effects are considered. For evaporation above an isothermal surface the droplet temperature exceeds the wet-bulb temperature corresponding to evaporation in an unbounded ambience during evaporation, then asymptotically approaches the infinite medium wet-bulb temperature. In the potential flow limit, the numerical results were in agreement with the analytical potential flow solution to this problem.

Acknowledgments—Conversations with Dr W. R. C. Phillips, Prof. P. C. T. de Boer, and Mr S. Chandra of Cornell University have been helpful. This work was supported by the National Science Foundation through grant No. CBT-8451075. Computational work was performed on the Cornell Theory Center Production Supercomputer Facility.

REFERENCES

1. B. S. Gottfried, C. J. Lee and K. J. Bell, The Leidenfrost phenomenon: film boiling of liquid droplets on a flat plate, *Int. J. Heat Mass Transfer* **9,** 1167–1187 (1966).
2. B. S. Gottfried and K. J. Bell, Film boiling of spheroidal droplets, *Ind. Engng Chem. Fundam.* **5,** 561–568 (1966).
3. M. Mizomoto, S. Ikai and A. Morita, Evaporation and ignition of a fuel droplet on a hot surface (part 4, model of evaporation and ignition), *Comb. Flame* **51,** 95–104 (1983).
4. C. T. Avedisian, C. Ioffredo and M. J. O'Connor, Film boiling of discrete droplets of mixtures of coal and water on a horizontal brass surface, *Chem. Engng Sci.* **39,** 319–327 (1984).
5. C. T. Avedisian and J. Koplik, Leidenfrost boiling of methanol droplets on hot porous/ceramic surfaces, *Int. J. Heat Mass Transfer* **30,** 379–393 (1987).
6. P. Cho and C. K. Law, Pressure/temperature ignition limits of fuel droplet vaporizing over a hot plate, *Int. J. Heat Mass Transfer* **28,** 2174–2176 (1985).
7. M. A. Goldshtik, V. M. Khanin and V. G. Ligai, A liquid drop on an air cushion as an analogue of Leidenfrost boiling, *J. Fluid Mech.* **166,** 1–20 (1986).
8. M. Fatchi, M.S. Thesis, Cornell University (1986).
9. A. K. Sen and C. K. Law, On a slowly evaporating droplet near a hot plate, *Int. J. Heat Mass Transfer* **27,** 1418–1421 (1984).
10. Z. Tamura and Z. Tanasawa, Evaporation and combustion of a drop contacting with a hot surface, 7th Symp. (Int.) Comb., pp. 509–522 (1959).
11. M. Kistemaker, The spheroidal state of a water drop, *Physica* **29,** 96–104 (1963).
12. C. K. Law, Recent advances in droplet vaporization and combustion, *Prog. Energy Comb. Sci.* **8,** 171–201 (1982).
13. K. J. Baumeister, T. D. Hamill and G. J. Schoessow, A generalized correlation of vaporization times of drops in

film boiling on a flat plate, *Proc. 3rd Int. Heat Transf. Conf.*, Chicago, Vol. 4, pp. 66–73 (1966).
14. S. Goldstein, *Modern Developments in Fluid Dynamics*, Vol. 1, pp. 114–115. Dover, New York (1965).
15. N. N. Lebedev, *Special Functions and their Applications*, pp. 230–234. Dover, New York (1972).
16. R. C. Reid, J. M. Prausnitz and T. K. Sherwood, *The Properties of Gases and Liquids*, 3rd Edn. McGraw-Hill, New York (1977).
17. R. T. Tal, D. N. Lee and W. A. Sirignano, Heat and momentum transfer around a pair of spheres in viscous flow, *Int. J. Heat Mass Transfer* **27**, 1953–1962 (1984).
18. E. M. Twardus and T. A. Brzustowski, The interaction between two burning droplets, *Archwm Thermodyn.* **8**, 347–358 (1977).
19. A. Umemura, S. Ogawa and N. Oshima, Analysis of the interaction between two burning droplets, *Comb. Flame* **41**, 45–55 (1981).

APPENDIX A

An analytical solution to the quasi-steady Leidenfrost evaporation problem for spherical droplets on an adiabatic surface can be obtained in the limiting case of neglect of both the viscous term in equation (4) and transient droplet heating, and for a Lewis number of unity. The solution is then similar to that previously published for two droplets evaporating or burning in an unbounded ambience and separated by a known distance [18, 19]—a so-called tandem droplet problem. Prior solutions to the tandem droplet problem have assumed that the interdroplet spacing (or what would equivalently be the levitation height in the Leidenfrost problem) is constant during evaporation. This assumption is not valid for the Leidenfrost problem as the levitation height must continuously change during evaporation to satisfy the force balance around the droplet. The value of the potential flow solution to the Leidenfrost problem for spherical droplets resides in checking the accuracy of the numerical method employed for solving the full problem.

The equations to be solved are equations (3), (5), and (6), together with the equation for the velocity potential

$$\nabla^2\phi = 0 \tag{A1}$$

where

$$\nabla\phi = \rho_v \mathbf{V}. \tag{A2}$$

Equations (24) and (27) under the potential flow assumption can be written as

$$-\frac{1}{2\rho_v}\int(\nabla\phi\cdot\nabla\phi)\mathbf{n}\cdot\mathbf{j}\,d\sigma = \frac{4}{3}\pi R^3 g(\rho_l-\rho_v) \tag{A3}$$

and

$$\int \mathbf{n}\cdot\nabla\phi\,d\sigma = -\frac{4}{3}\pi\rho_l\frac{d(R^3)}{dt}. \tag{A4}$$

The energy and species conservation equations may be coupled by defining

$$b \equiv \frac{C_v(T_\infty - T)}{h_{fg}} = \frac{Y_l}{1-Y_{ls}} \tag{A5}$$

so that equations (5) and (6) become

$$\mathbf{V}\cdot\nabla b = \frac{k}{C_v}\nabla^2 b. \tag{A6}$$

The boundary conditions for equations (A1) and (A6) are

$$\frac{\partial b}{\partial n} = \frac{\partial\phi}{\partial n} = 0 \text{ at } \beta = 0 \tag{A7}$$

$$b = B,\ \phi = \phi_l \text{ at } \beta = \beta_0 \tag{A8}$$

$$b = \phi = 0 \text{ at } \alpha = \beta = 0. \tag{A9}$$

The particular solution to equations (A6)–(A9) is

$$b = B\frac{1-\exp[\phi C_v/k]}{1-\exp[\phi_l C_v/k]} \tag{A10}$$

where

$$B = \frac{C_v(T_\infty - T_s)}{h_{fg}} \tag{A11}$$

and

$$\phi_l = -\frac{k}{C_v}\ln(1+B). \tag{A12}$$

The solution for the velocity potential via separation of variables is

$$\phi = \phi_l\sqrt{2}(\cosh\beta - x)^{1/2}\sum_{n=0}^{\infty} P_n e^{-(n+1/2)\beta_0} \times \frac{\cosh[(n+1/2)\beta]}{\cosh[(n+1/2)\beta_0]} \tag{A13}$$

where $x = \cosh\alpha$ and P_n are Legendre polynomials of the first kind of degree n. Equations (A3) and (A4) can now be written as

$$R^2 = \left[\frac{3}{2}\frac{\phi_l^2}{g\rho_v(\rho_l-\rho_v)}\right]^{2/3} I^{2/3} \tag{A14}$$

and

$$\frac{dR^2}{dt} = -2\frac{|\phi_l|}{\rho_l}\sinh\beta_0\sum_{n=0}^{\infty}\frac{e^{-(n+1/2)\beta_0}}{\cosh[(n+1/2)\beta_0]} \tag{A15}$$

where

$$I(\beta_0) = \int_{-1}^{1} f(x,\beta_0)\,dx \tag{A16}$$

and

$$f(x,\beta_0) = (x\cosh\beta_0 - 1)\cdot\left[\sum_{n=0}^{\infty} P_n e^{-(n+1/2)\beta_0} \times (n+1/2)\tanh[(n+1/2)\beta_0] + 1/2(\cosh\beta_0 - x)^{-1} \times \sinh\beta_0\sum_{n=0}^{\infty} P_n e^{-(n+1/2)\beta_0}\right]^2. \tag{A17}$$

Equations (A14) and (A15) combine to yield the evolution of β_0, hence droplet radius and evaporation time ($\beta_0 \to \infty$), as

$$t = -\left[\frac{12g^2\rho_v^2(\rho_l-\rho_v)^2}{\rho_l^3|\phi_l|}\right]^{1/3} \times \int_{\beta_i}^{\beta_0}\frac{dI/d\beta_0}{I^{1/3}\sinh\beta_0\sum_{n=0}^{\infty}\frac{e^{-(n+1/2)\beta_0}}{\cosh[(n+1/2)\beta_0]}}d\beta_0 \tag{A18}$$

where δ and A will be as defined in equations (11) and (12). The initial value of β in equation (A18)—β_i—is determined from equation (A14) by setting $R = R_i$ (the initial droplet radius) and then solving for $\beta_0 \to \beta_i$ together with equations (A16) and (A17).

Predictions of evaporation time and droplet radius are exact if equations (A16)–(A18) can be integrated analytically. However, no analytical evaluation of I, and hence t in equation (A18), exists. The function $f(x,\beta_0)$ defined by equation (A17) is particularly difficult to integrate for small β_0. Predictions from the potential flow solution must then be recognized as involving some degree of numerical inaccuracy. This inaccuracy is minimized for the range of initial droplet sizes, and hence values of β_i, considered here.

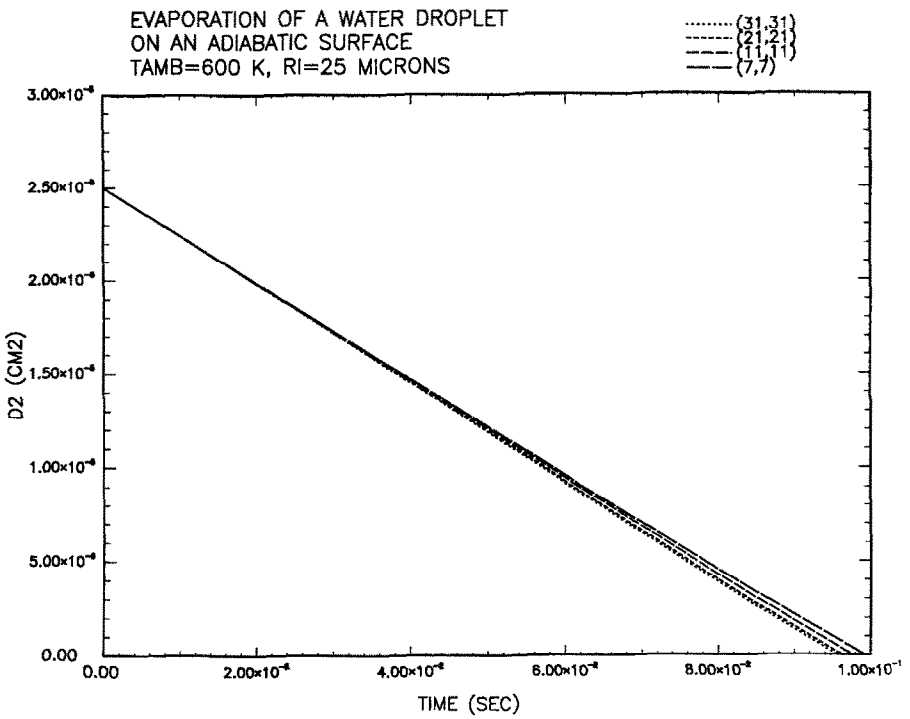

FIG. A1. Effect of grid spacing on calculated steady state evolution of droplet diameter (d^2) and total evaporation time [$t(d^2 = 0)$] for a water droplet at an adiabatic surface. $T_\infty = 600$ K, $T_s = T_{s0} = 300$ K, $R_i = 25\,\mu$m. ····, 31×31; ----, 21×21; – – –, 11×11; ———, 7×7.

The question of accuracy of the numerical solution is now addressed in two parts: one relates to convergence of the numerical scheme as grid spacing is reduced, and the other concerns the accuracy of the numerical method itself (i.e. is the solution correct or physically meaningful?). The two questions are interconnected: in principle for a fine enough grid spacing the converged solution is also accurate. The question of accuracy is best answered by comparison with a related analytical solution. The solution used for this purpose is from the potential flow problem described above.

Figure A1 shows the effect of grid spacing (in the α–η plane) on the evolution of diameter squared. For these calculations, droplet heating was neglected. It is evident that as the grid becomes finer, convergence occurs; it is also true that the computational time increases substantially. For example convergence required about 4 h of computational time on an IBM 4381 for the 31×31 grid, but only about 1 h for the 21×21 grid. The small differences shown in Fig. A1 justify using the 21×21 grid to generate the results discussed in Section 4.

Figure A2 compares the analytical potential flow solution with the solution obtained by setting $\mu = 0$ in the discretized form of equations (11)–(27) (for case II). For this purpose the variation of d^2 with time is used as a basis of comparison. The numerical solution again neglected droplet heating, as the analytical solution only applies for this case. The very small differences in diameter squared in the two solutions shown in Fig. A2 are indicative of the accuracy of the numerical solution. Differences in the total evaporation time (corresponding to $d^2 = 0$) are also very small as shown in Fig. A2. The close agreement between the analytical and numerical solutions is thus indicative of the accuracy of the numerical method employed in the calculations presented in Figs. 2–7 and A1.

APPENDIX B

Two possible sources for internal circulation within a droplet evaporating near a wall are the following: (1) an external non-radial flow which creates a shear stress at the droplet surface, and (2) surface tension gradients.

The existence of surface tension gradients is specifically ruled out by the assumption of a spatially uniform droplet temperature. For the small droplets considered in this study, on the order of 50 μm diameter, this assumption is valid.

An external non-radial flow around the droplet can be created in three ways. In the first, the gas phase temperature difference between the droplet, ambience, and wall could create a buoyancy induced flow around the droplet. To assume buoyancy effects can be neglected requires demonstrating that the evaporation induced (i.e. Stefan) flow is much greater than the buoyancy induced gas flow. For this purpose a characteristic free convective velocity is defined through an order of magnitude analysis on the momentum equation by equating the buoyancy term with the inertia term

$$V_b \sim [g\kappa\Delta T d]^{1/2} \tag{B1}$$

where κ is the isothermal compressibility. An order of magnitude of the evaporation induced velocity at the droplet surface is

$$V_e \sim \frac{\alpha_v \ln(1+B)}{d}. \tag{B2}$$

Free convection is taken to be negligible if $V_b/V_e \ll 1$. Assuming $d \sim 50\,\mu$m, and typical orders of magnitude for the fluids studied of $\alpha_v \sim 0.1$ cm^2 s^{-1}, $\kappa \approx 10^{-4}k^{-1}$, $B \sim 1$, and $\Delta T \sim 200$ K we find that $V_b/V_e \sim 0.02$. For larger droplets, free convective flow around the droplet may be important. This flow may give rise to the complications leading to oscillatory motion of larger droplets. As evaporation proceeds and the droplet gets smaller such oscillations disappear. Oscillations generally do not occur for droplets on the order of less than about 1 mm diameter, thus demonstrating the possible reduced influence of buoyancy induced flow for smaller droplets.

A second source of a tangential velocity at the droplet

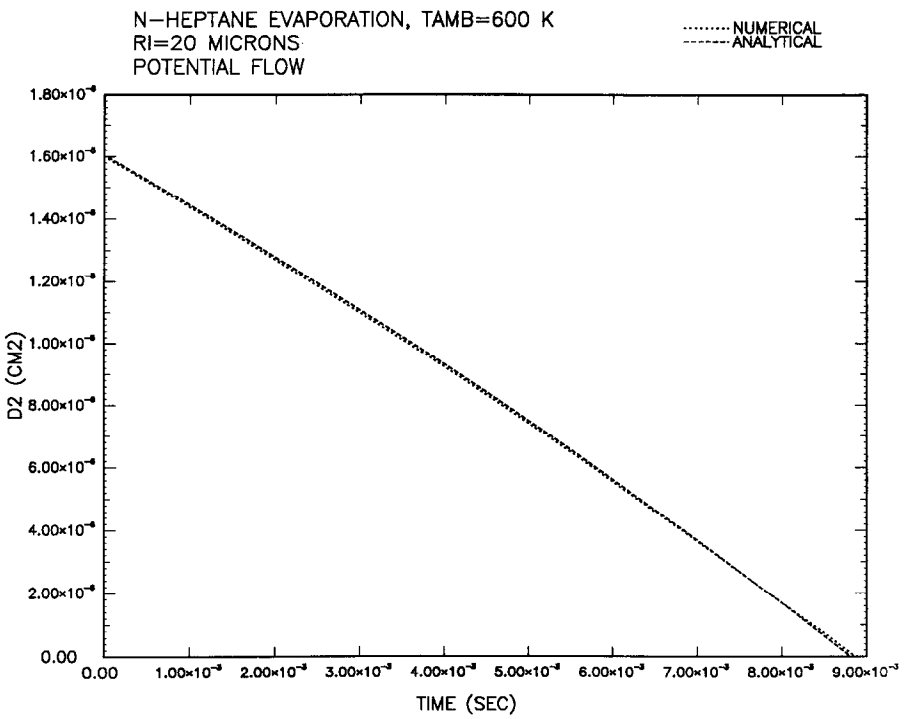

FIG. A2. Comparison between numerical (····) and analytical (----) potential flow solution for steady state n-heptane droplet evaporation at an adiabatic surface. $T_\infty = 600$ K, $R_i = 20$ μm.

surface is conjectured to come from the evaporation process itself. Streamlines emerging from the droplet must bend due to the presence of the wall. The extent of their curvature is governed by the magnitude of the vaporization rate and droplet levitation height. Streamlines originating from the lower hemisphere of the droplet could in principle bend around the droplet even in the absence of free convective motion to the extent that along the upper surface of the droplet there is a non-zero tangential velocity, and hence shear stress. The neglect of the attendant liquid motion is contingent on the characteristic time for liquid motion being much longer than the characteristic time for droplet evaporation. An order of magnitude estimate for the liquid velocity within the droplet is obtained by assuming that shear is continuous across the gas/liquid interface. Hence, to an order of magnitude

$$V_l \sim \frac{D}{\mu_l}\tau_v \tag{B3}$$

where a characteristic dimension in the liquid has been taken as the droplet diameter. The characteristic time (for a particle to traverse the droplet circumference) for liquid circulation is approximately

$$t_l \sim \frac{\mu_l}{\tau_v}. \tag{B4}$$

An order of magnitude for the droplet regression time is obtained with the aid of equation (B2) as

$$t_{reg} \sim \frac{\rho_l}{\rho_g}\frac{d^2}{\alpha_v \ln(1+B)}. \tag{B5}$$

We neglect internal circulation if $t_l/t_{reg} \gg 1$. To estimate τ_v we use values from the numerical analysis discussed in Sections 3 and 4 which neglected liquid motion, believing that τ_v, and hence V_l, would be less if internal circulation were included in the analysis. From our numerical results, τ_v ($= \tau_{\alpha\beta}$ from equation (25)) $\sim 10^{-3}$ g cm^{-1} s^{-2}. For $\alpha_v \sim 0.1$ cm s^{-2}, $d \sim 50$ μm, $\rho_l/\rho_v \sim 1000$ and $\mu_l \sim 0.1$ g cm^{-1} s^{-1} we find that $t_l/t_{reg} \sim 277$. Since $t_l/t_{reg} \sim 1/d^2$, internal circulation could become an important effect to consider for larger droplets.

A third source for a non-radial flow at the droplet surface could be created by the progressive motion of the droplet away from the surface as it evaporates (cf. Fig. 6). This motion is due to temporal variations of levitation height. It creates an effective motion around the droplet which is similar to a droplet placed in a uniform convective free stream moving at a velocity of $\partial\delta/\partial t$. The external Reynolds number in this situation provides a measure of the extent to which internal circulation must be considered to correctly model the evaporation process.

Defining V_δ as a free stream gas velocity, the effective free stream Reynolds number is $Re = V_\delta d/\nu$ where $V_\delta = \partial\delta/\partial t$. V_δ was estimated from the present calculations to range between about 0.06 cm s^{-1} as $t \to 0$ to a maximum of about 1 cm s^{-1} as $t \to t_e$. Taking $d = 50$ μm and $\nu \sim 0.1$ cm^2 s^{-1} we have that $0.003 < Re < 0.05$. At these small Reynolds numbers, movement of the droplet caused by temporal variations of levitation height, and the attendant possible liquid circulation, is not expected to exert a strong influence on the evaporation rate.

SOLUTION NUMERIQUE DE L'EVAPORATION EN FILM D'UNE GOUTTELETTE LIQUIDE SPHERIQUE SUR UNE SURFACE ISOTHERME OU ADIABATIQUE

Résumé—On présente une solution numérique du problème de l'évaporation en film d'une gouttelette liquide sur une surface horizontale. Les gouttelettes sont suffisamment petites pour être supposées sphériques. Deux cas sont considérés: (1) la surface est maintenue à une température constante (cas I), et (2) la surface est isolée tandis que l'ambiance est chaude (cas II). Le système complet d'équations est résolu pour les hypothèses suivantes: (1) l'évaporation est quasi permanente, (2) il n'y a pas de circulation interne du liquide, (3) les propriétés thermophysiques sont constantes, et (4) la température de la goutte est spatialement uniforme mais variable dans le temps. Le nombre de Lewis n'est pas supposé être égal à l'unité; les effets de viscosité de la phase gazeuse, la convection de type Stefan et l'inertie de la phase gazeuse sont inclus dans l'analyse. Le temps de l'évaporation totale de la goutte diminue quand augmente la température de la plaque ou de l'ambiance et la goutte s'écarte progressivement de la plaque quand elle s'évapore. Les résultats numériques s'accordent avec la solution analytique de l'évaporation en film d'une gouttelette sur une surface adiabatique dans le cas des grands nombres de Reynolds effectifs (écoulement potentiel).

EINE NUMERISCHE LÖSUNG FÜR DIE FILMVERDAMPFUNG EINES KUGELIGEN FLÜSSIGKEITSTROPFENS AN EINER ISOTHERMEN, ADIABATEN OBERFLÄCHE

Zusammenfassung—Es wird eine numerische Lösung für das Problem der Filmverdampfung eines Flüssigkeitstropfens an einer horizontalen Oberfläche vorgestellt. Die Tropfen sind klein genug um als kugelig angenommen werden zu dürfen. Zwie prizipielle Fälle werden betrachtet: Fall I: Die horizontale Oberfläche wird auf konstanter Temperatur gehalten; Fall II: Die Oberfläche ist isoliert, während die Umgebung heiß ist. Der komplette Satz der Gleichungen, die dieses Problem beschreiben, wird unter den folgenden Annahmen gelöst: (1) Die Verdampfung ist quasi-stationär, (2) Keine interne Flüssigkeitszirkulation, (3) Konstante Stoffwerte und (4) Die Tropfentemperatur ist räumlich konstant aber zeitlich veränderlich. Es wird nicht angenommen, daß die Lewis-Zahl gleich Eins ist. Viskositätseffekte der Gasphase, Konvektion vom Stefan-Typ und die Trägheit der Gasphase werden in der Untersuchung berücksichtigt. Wie erwartet, verkürzt sich die Zeit bis zur vollständigen Verdampfung des Tropfens mit steigender Platten(I)-bzw. Umgebungs(II)temperatur. Der Tropfen bewegt sich deutlich von der Platte weg, wenn er verdampft. Die numerischen Ergebnisse stimmen im Bereich großer effektiver Reynolds-Zahlen (speziell bei Potentialströmung) gut mit der analytischen Lösung für die Filmverdampfung eines Tropfens über einer adiabaten Oberfläche in heißer Umgebung überein.

ЧИСЛЕННОЕ РЕШЕНИЕ ЗАДАЧИ ПЛЕНОЧНОГО ИСПАРЕНИЯ СФЕРИЧЕСКОЙ ЖИДКОЙ КАПЛИ НА ИЗОТЕРМИЧЕСКОЙ И АДИАБАТИЧЕСКОЙ ПОВЕРХНОСТЯХ

Аннотация—Получено численное решение задачи пленочного испарения жидкой капли на горизонтальной поверхности. Небольшие размеры капель оправдывают допущение об их сферичности. Рассматриваются два принципиальных случая: (1) температура горизонтальной поверхности постоянна (случай I) и (2) поверхность теплоизолирована от нагретой среды (случай II). Для этой задачи решена полная система определяющих уравнений при следующих допущениях: (1) испарение квазистационарное; (2) отсутствует внутренняя циркуляция жидкости; (3) овойства постоянны; (4) температура капли постоянна в пространстве, но изменяется во времени. Число Льюиса принимается неравным единице. Рассматриваются вязкие эффекты газовой фазы, конвекция по закону Стефана, учтена инерция газовой компоненты. Как и ожидалось, общее время испарения капли уменьшается с ростом температуры пластины (I) или окружающей среды (II), а капля по мере ее испарения все больше удаляется от пластины. Получено хорошее соответствие численных результатов с аналитическим решением для задачи пленочного испарения капли над адиабатической поверхностью в сильно нагретой среде при больших эффективных числах Рейнольдса (случай потенциального течения).